https://doi.org/10.5194/egusphere-2026-1715
Preprint. Discussion started: 27 March 2026

A Study of Pre-earthquake Anomalies in Geomagnetic and Borehole Strain Data Based on the Pyraformer Model

Jie Zhang[1,2], Minhao Sun[1,2], Changfeng Qin[1,2], Feng Mu[1,2], Shanzhi Dong[1,2], Yu Duan[1,2], Dewang Zhang[1,2], Chengquan Chi[1,2]

[1]School of Artificial Intelligence, Hainan Normal University, Haikou, 571158, China
[2]Key Laboratory of Data Science and Smart Education, Hainan Normal University, Ministry of Education, Haikou, China

Correspondence to: Chengquan Chi (chicq@hainnu.edu.cn) and Dewang Zhang (zhangdwsan@163.com)

Abstract. As a major natural hazard, earthquakes are accompanied by lithospheric stress accumulation and anomalies in multiple physical fields during their preparation process. Identifying pre-earthquake anomalies is therefore of great scientific significance for understanding earthquake preparation and improving earthquake prediction. Taking the 2013 Lushan earthquake in Sichuan, China (Ms 7.0), as a case study, this work presents a comprehensive analysis of geomagnetic and borehole strain observations to investigate the spatiotemporal evolution of pre-earthquake multi-physical-field anomalies. First, Variational Mode Decomposition (VMD) was applied to geomagnetic and borehole strain data to achieve multi-scale signal decomposition, thereby separating long-term background variations from short-period disturbance components. Subsequently, the Pyraformer model was employed to model and predict the high-frequency feature sequences, and the prediction residuals were extracted to quantify pre-earthquake anomalies. The results show that borehole strain anomalies first emerged along local fault segments during the pre-seismic stage and gradually accumulated, whereas geomagnetic anomalies subsequently intensified and accelerated at adjacent stations. Overall, the anomalies exhibited a spatiotemporal evolution pattern characterized by local-to-regional expansion and stage-wise accelerated accumulation. Further analysis indicates that borehole strain anomalies generally preceded geomagnetic anomalies, with a time lag ranging from several days to several weeks between the rapid accumulation stage of borehole strain anomalies and the strengthening stage of geomagnetic anomalies. In addition, the cumulative anomaly curves commonly displayed a pronounced S-shaped growth pattern, reflecting the gradual increase in stress-strain during earthquake preparation and its subsequent transfer to the electromagnetic field response. These findings reveal a coupling relationship between the stress-strain field and the electromagnetic field during the earthquake preparation process. The integrated VMD-Pyraformer framework proposed in this study demonstrates strong stability and reliability in identifying geomagnetic and borehole strain anomalies and provides new observational evidence and an effective analytical approach for multi-station, multi-parameter joint monitoring and pre-earthquake anomaly identification.

Keywords: Pre-earthquake anomalies; Pyraformer; Multi-source observation; Anomaly extraction

https://doi.org/10.5194/egusphere-2026-1715
Preprint. Discussion started: 27 March 2026

1 Introduction

Earthquakes are major geological hazards driven by dynamic processes within the Earth. Their occurrence is mainly attributed to stress accumulation resulting from the collision, rifting, and shearing of tectonic plates within the lithosphere (Liu, 2024). In addition to causing direct damage to surface structures, infrastructure, and landforms, earthquakes may also trigger a series of secondary disasters, including fires, landslides, floods, hazardous chemical leaks, and infectious disease outbreaks (Chen et al., 2012; Yang and Zhao, 2014). As one of the most destructive natural hazards, earthquakes often result in significant casualties and severe economic losses. Therefore, investigating anomalous phenomena that may arise prior to earthquakes is of great scientific significance for understanding pre-seismic processes and enhancing earthquake risk mitigation capabilities.

A systematic investigation of earthquake precursor observations is of considerable scientific significance for deepening our understanding of earthquake generation processes and their potential impacts. By analyzing the spatiotemporal patterns and evolutionary characteristics of multi-source observational data, anomalous signals associated with pre-earthquake processes can be identified. Existing studies have employed a variety of observational approaches, including ammonia concentration monitoring (Tsuchiya et al., 2024), variations in groundwater chemistry (Yang et al., 2021), changes in the dominant azimuth of the ground electric field (Hou et al., 2021), regional GPS deformation anomalies (Wang et al., 2020), perturbations in ionospheric electron density (De Santis et al., 2019), and thermal infrared remote sensing (Ouzounov et al., 2007). These multidisciplinary and multi-parameter studies provide important theoretical foundations and technical support for elucidating earthquake nucleation mechanisms and enhancing short-term earthquake forecasting capabilities.

With the establishment of the Plate Boundary Observatory (PBO) and the EarthScope programme, significant advances have been achieved in geomagnetic monitoring and borehole strain observation techniques. These initiatives have generated a large volume of high-quality geophysical observation data, which have been widely used in studies of slow earthquakes, microseismic activity, and stress–strain evolution processes (Gladwin, 1984; Gladwin and Hart, 1985; Barbour and Agnew, 2012). In the field of electromagnetic precursors, Gokhberg et al. (1982) reported that the preparation stage of major earthquakes may be accompanied by low-frequency electromagnetic anomalies. Akinaga et al. (2001) observed a significant increase in the polarisation ratio of Ultra-Low-Frequency (ULF) electromagnetic waves prior to an earthquake in Taiwan, indicating that low-frequency magnetic field disturbances may serve as detectable pre-seismic indicators. Han et al. (2014) proposed a cumulative energy index to characterise the statistical behavior of magnetic field disturbances and found that it exhibited a sustained upward trend before several major earthquakes. In addition, Zhu et al.(2020) employed skewness and kurtosis analyses to demonstrate that geomagnetic time series showed clear deviations from normality prior to earthquakes, suggesting systematic changes in their probability structure during the preparation stage. In research on stress- and strain-related precursors, Qiu et al. (1998) identified significant tensile stress pulse anomalies based on data from stress monitoring stations. Chi et al. (2013) detected tidal distortion strain anomalies in borehole strain observations that were closely associated with pre-seismic strain disturbances. Wu et al. (2012) simulated the evolution of the seismic system using a

https://doi.org/10.5194/egusphere-2026-1715
Preprint. Discussion started: 27 March 2026

cluster statistical equation and revealed its relationship with precursor anomalies. Furthermore, Tang et al. (2013) identified both compressional and extensional anomalies in the amplitudes of borehole strain records and suggested that these amplitudes may be related to earthquake magnitude. Collectively, these studies based on geomagnetic, stress, and strain monitoring demonstrate that multi-parameter observations can effectively reveal the physical processes involved in earthquake preparation, thereby providing important scientific evidence for short-term earthquake prediction.

In recent years, with the continuous growth of computing power and the rapid advancement of artificial intelligence, machine learning methods have been increasingly employed in seismic precursor anomaly detection and earthquake prediction research. In the field of geomagnetic data analysis, Huang et al. (2023) employed Convolutional Neural Networks (CNNs) for geomagnetic signal recognition and achieved automatic extraction of local short-term disturbance features prior to earthquakes. Abduallah et al. (2022) leveraged the global attention mechanism of Transformers to capture long-range dependencies in geomagnetic sequences, thereby improving the stability and generalisation performance of anomaly detection. Yu et al.(2024) further proposed the Transformer-based ATGM framework to analyse geomagnetic anomalies associated with three major earthquakes in the Sichuan region. In addition, several studies have incorporated Residual Networks (ResNet) (Zhang et al., 2025a), Spatio-Temporal Convolution (ST-Conv) (Lains, 2011), Covariance-Observations (COV-OBS) (Lains, 2011), and Wavelet-Convolutional Neural Networks (Wavelet-CNN) (Rabie et al., 2021) for multi-scale analysis of geomagnetic signals, thereby separating background noise from large-scale disturbances. In the analysis of strain and crustal deformation data, Chi et al. (2019) combined VMD with state-space modelling and Principal Component Analysis (PCA) to extract anomalous evolutionary characteristics prior to the Wenchuan earthquake. Yu et al.(2020) employed Multichannel Singular Spectrum Analysis (MSSA) to reveal coherent pre-seismic patterns in multi-station strain observations. Li et al.(2025) integrated VMD with a graph neural network（Graph WaveNet), to construct a spatiotemporally coupled prediction framework and identified the accumulation of anomalous signals prior to the Jiuzhaigou earthquake. In addition, Random Forest (RF) models (Akhoondzadeh, 2016; Asim et al., 2017; Tsuchiya et al., 2024), decision trees (Sikder and Munakata, 2009), Gated Recurrent Units (GRU) (Chi et al., 2023), and Long Short-Term Memory (LSTM) networks (Wang et al., 2017; Zhang and Wang, 2024) have also been widely applied in earthquake precursor identification research.

As research on earthquake precursors has progressed, it has become increasingly evident that reliance on a single station or a single observational parameter is insufficient to fully characterise the complex physical processes preceding earthquakes. Consequently, research has gradually shifted from single-station observations to multi-station collaborative analyses, and from single-parameter monitoring to multi-parameter joint analyses. Some studies have investigated regional crustal deformation by integrating borehole strain observations with Global Navigation Satellite System (GNSS) data, demonstrating that multi-source observations can provide a more comprehensive understanding of the evolution of pre-seismic strain (Fan et al., 2022). Meanwhile, studies based on the Lithosphere-Atmosphere-Ionosphere Coupling (LAIC) theory have revealed the propagation and coupling processes of pre-seismic anomalous signals across the lithosphere, atmosphere, and ionosphere through the integrated analysis of diverse observational datasets, including electromagnetic signals, ionospheric electron density, and atmospheric parameters (Hayakawa and Hobara, 2024; Zhang et al., 2024).

https://doi.org/10.5194/egusphere-2026-1715
Preprint. Discussion started: 27 March 2026

Furthermore, multi-source joint inversion approaches, such as the combined inversion of seismic and electromagnetic data, have been proposed to improve the reliability and stability of subsurface structure interpretation (Ma et al., 2025). Collectively, these studies indicate that joint analyses involving multiple stations and parameters can more comprehensively characterise the evolution of pre-earthquake anomalies, thereby providing a more reliable observational basis for earthquake precursor identification and prediction.

This study proposes an integrated VMD-Pyraformer framework for extracting pre-seismic anomaly signals from geomagnetic and borehole strain observations. The proposed method is designed to leverage the multi-scale decomposition capability of VMD and the strength of Pyraformer in long-sequence modelling, thereby enabling effective identification of potential pre-seismic anomalies. The overall workflow of the study is illustrated in Figure 1. First, the raw geomagnetic and borehole strain observation sequences are decomposed using VMD. By retaining informative modes and fusing the corresponding components, the influence of background signals, such as interannual variations and solid tides, is reduced, thereby enhancing the detectability of local pre-seismic disturbances. Subsequently, the fused feature sequences are input into the Pyraformer model for training and prediction to extract anomalous evolutionary patterns potentially associated with earthquake preparation. Finally, statistical analyses are conducted on the cumulative changes in pre-earthquake anomalies at each station to characterise the disturbance evolution from multiple perspectives.

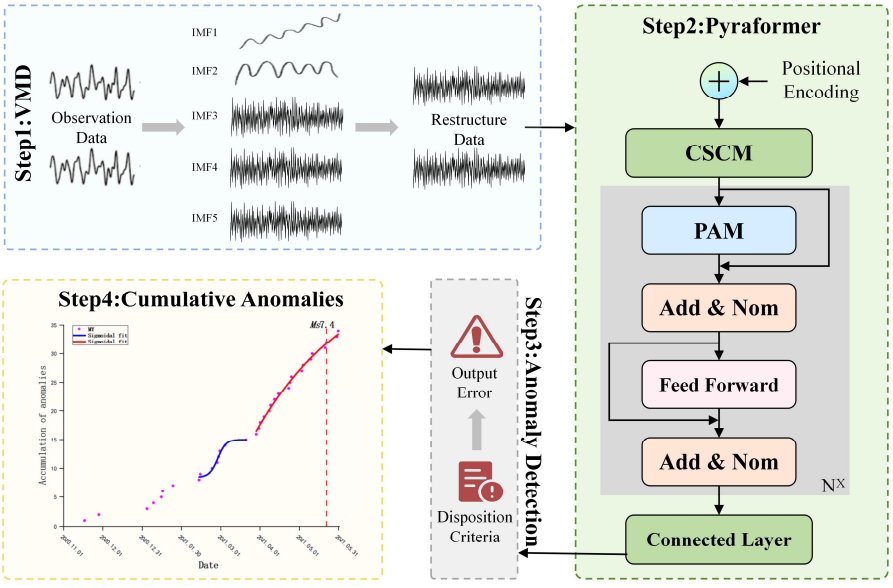

Figure 1: Overall Research Flowchart.

https://doi.org/10.5194/egusphere-2026-1715
Preprint. Discussion started: 27 March 2026

2 Observation Data and Earthquake Cases

2.1 Geomagnetic Data

The geomagnetic field is one of the fundamental geophysical fields of the Earth, with a spatial distribution extending from the Earth's interior into near-Earth space and forming a vector field that varies in both time and space (Cui, 2021). Earthquake generation is closely related to the continuous accumulation and redistribution of tectonic stress within the crust, a process that is often accompanied by disturbances in the electromagnetic environment and anomalous radiation phenomena. Consequently, geomagnetic monitoring has become one of the key technical approaches for investigating pre-earthquake electromagnetic anomalies (Wang et al., 2025). At present, China has established hundreds of geomagnetic observation stations in several seismically active regions to monitor earthquake-related electromagnetic disturbances. These instruments record two orthogonal horizontal components (N–S and E–W) and one vertical component (Z), providing high-precision and high-resolution measurements of geomagnetic field intensity at different sampling rates. The output voltage of the instrument is linearly related to the magnetic field intensity (Heinecke, 2007):

$$B = K \cdot V + B_0 , \tag{1}$$

$$\begin{cases} X_{(N-S)} = K_x V_x + X_0 \\ Y_{(E-W)} = K_y V_y + Y_0 \\ Z \quad\quad\;\; = K_z V_z + Z_0 \end{cases} , \tag{2}$$

where, B denotes the magnetic field component (X/Y/Z), V denotes the sensor output voltage, K represents the proportional coefficient, and B_0 denotes the zero offset. The vertical component (Z) of the geomagnetic field is highly sensitive to space weather phenomena, such as geomagnetic storms and ionospheric disturbances, and is also more effective in reflecting magnetic disturbances associated with deep current system activity and crustal stress changes in mid- to low-latitude regions. Therefore, the vertical geomagnetic component (Z) recorded at the Chengdu, Xichang, and Muli stations was selected in this study as the core observational parameter for pre-earthquake anomaly identification and modelling.

2.2 Borehole Strain Data

With the continuous advancement of crustal deformation monitoring technology, four-component borehole strain observation systems have been continuously refined and have become one of the key technical tools for identifying pre-seismic anomalies and investigating the earthquake-generation process (Qiu et al., 2015). The YRY-4 four-component borehole strainmeter, developed in China, is characterised by high sensitivity, wide-band response, and long-term operational stability. It is capable of continuously recording minute displacement variations at observation sites at a minute-level sampling interval, thereby allowing the microscale strain evolution of subsurface media to be inferred. This instrument simultaneously records four independent strain components, denoted as S_1, S_2, S_3 and S_4, where S_1 represents the reference direction and the other three measurement directions are arranged sequentially. The combined observations from these four

https://doi.org/10.5194/egusphere-2026-1715
Preprint. Discussion started: 27 March 2026

components can be used to derive the orientations of the principal strain axes and the corresponding principal strain values (Qiu et al., 2009; Su, 2019):

$$S_1 + S_2 = k(S_3 + S_4), \tag{3}$$

this equation is used for the self-calibration of four-component borehole strainmeters. When $k \geq 0.95$, the data recorded by the four directional strain components are considered to exhibit good compatibility and stability, indicating that the measurement results are reliable. Under approximate plane-strain conditions at or near the Earth's surface, only three of the four strain components observed by a four-component strainmeter are linearly independent. Therefore, in practical analyses, three independent components are typically selected for subsequent processing and modelling (Chi, 2020):

$$\begin{cases} S_{13} = S_1 - S_3 \\ S_{24} = S_2 - S_4 \\ S_a = (S_1 + S_2 + S_3 + S_4)/2 \end{cases}, \tag{4}$$

where, S_{13} and S_{24} denote independent shear strains, which describe deformation associated with changes in shape under conditions of constant area or volume. S_a denotes surface strain, which primarily characterises changes in unit area rather than shape and is commonly used to describe the accumulation of principal strain during crustal deformation. Compared with shear strain, surface strain provides a more comprehensive reflection of the strain responses across all four measurement directions and is more sensitive to the overall deformation state. Therefore, surface strain (S_a) data from the Kangding and Xiaomiaotai borehole strain stations were selected in this study as the primary observational parameters for pre-earthquake anomaly identification and modelling.

2.3 Lushan Earthquake

According to the China Earthquake Networks Center (CENC), a magnitude 7.0 earthquake struck Lushan County, Ya'an City, Sichuan Province, at 08:02 Beijing Time on 20 April 2013. The epicentre was located at 103.0°E and 30.3°N, with a focal depth of 13 km. The earthquake occurred in the region between the Dachuan–Shuangshi Fault Zone and the Xinkaitian Fault Zone, which is characterised by complex tectonic settings and represents one of the most seismically active tectonic zones in Sichuan Province (Wang et al., 2019). After the mainshock, aftershock activity increased markedly. By 00:00 on 21 April, a total of 6 aftershocks with $M_S \geq 5.0$ and 54 aftershocks with $M_S \geq 4.0$ had been recorded. This event caused severe casualties and extensive infrastructure damage, significantly affecting regional socioeconomic activities (Fang et al., 2015).

According to the empirical formula for the pre-earthquake influence radius proposed by Dobrovolsky, $D = 10^{0.43M}$ km, where M denotes the earthquake magnitude (Dobrovolsky et al., 1979). For an earthquake with Ms 7.0, the estimated earthquake preparation radius is 1,023.29 km. On this basis, data from the Chengdu, Xichang, and Muli geomagnetic observation stations, together with those from the Kangding and Xiaomiao borehole strain observation stations, were selected for the extraction and comprehensive analysis of pre-earthquake anomalies associated with the Lushan earthquake.

https://doi.org/10.5194/egusphere-2026-1715
Preprint. Discussion started: 27 March 2026

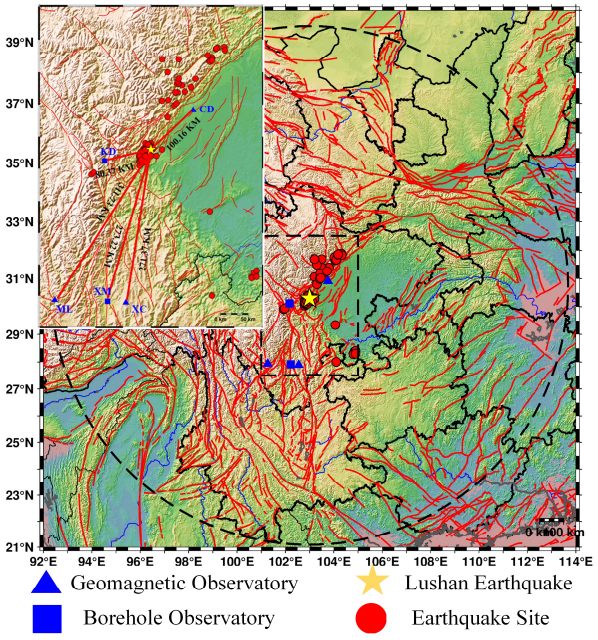

Figure 2: Map showing the distances between the earthquake epicenter and observation stations.

Geomagnetic Observatory				
Station Name	Longitude	Latitude	Distance	Sampling Rate
Chengdu	103.76	30.91	100.16	1 minute
Xichang	102.55	27.89	271.37	1 minute
Muli	101.272	27.932	311.73	1 minute
Borehole Strain Observatory				
Station Name	Longitude	Latitude	Distance	Sampling Rate
Kangding	102.17	30.12	80.37	1 minute
Xiaomiao	102.22	27.91	273.22	1 minute

Table 1: Observation Station Information

3 Research Methods

3.1Variational Mode Decomposition (VMD)

Dragomiretskiy et al. (2013) proposed a non-recursive and fully adaptive signal decomposition method, namely Variational Mode Decomposition (VMD), which has shown good robustness in processing complex signals characterised by nonlinearity, non-stationarity, and noise interference. VMD is based on classical Wiener filtering theory and the Fourier-domain analysis framework. By constructing and solving a constrained variational optimisation problem, it reformulates

https://doi.org/10.5194/egusphere-2026-1715
Preprint. Discussion started: 27 March 2026

signal decomposition as the search for an optimal solution with minimum bandwidth. In this way, the original signal is decomposed into a set of band-limited Intrinsic Mode Functions (IMFs) with finite bandwidths and non-overlapping centre frequencies. The variational model is expressed as follows:

$$\begin{cases} \min\limits_{\{u_k\},\{\omega_k\}} \sum_{k=1}^{K} \left\| \partial_t \left\{ \left[\left(\delta(t) + \frac{j}{\pi t} \right) * u_k(t) \right] e^{-j\omega_k t} \right\} \right\|_2^2, \\ st \sum_{k=1}^{K} u_k(t) = f(t) \end{cases} \tag{5}$$

where, $\{u_k\}$ and $\{\omega_k\}$ denote the decomposed modes and their corresponding centre frequencies, respectively, ∂_t denotes the temporal derivative with respect to time t, $\delta(t)$ is the unit impulse function, and j represents the imaginary unit. Compared with Empirical Mode Decomposition (EMD) and its improved variants, such as Ensemble Empirical Mode Decomposition (EEMD), Variational Mode Decomposition (VMD) has a more well-defined objective function and superior numerical stability, and can effectively alleviate problems such as mode mixing and end effects. In this study, VMD is applied to perform multi-scale decomposition of the vertical geomagnetic component (Z) and the surface strain (S_a) series obtained from borehole strain observations. Considering the physical characteristics of different observation variables, tailored data-processing strategies are adopted in subsequent modelling. For the geomagnetic Z component, the high-frequency modes obtained from the decomposition are selected to emphasise short-term disturbance features prior to the earthquake. For the borehole strain S_a data, long-term trend components are first removed, after which the remaining medium- and high-frequency information is used for modelling and analysis, thereby enhancing the ability to characterise the evolution of pre-earthquake anomalies.

3.2 Pyraformer Neural Network

In recent years, deep learning methods have been widely applied to seismic signal identification and prediction research, providing new technical tools for modelling and analysing complex seismic processes. Existing studies have achieved substantial progress in time-series forecasting using models such as LSTM, GRU, and Transformers. However, these models still exhibit certain limitations in Long-Sequence Time-series Forecasting (LSTF) tasks. On the one hand, traditional recurrent architectures are prone to information loss when modelling long-range dependencies. On the other hand, models based on global attention mechanisms often entail high computational complexity, which limits their applicability to ultra-long sequence scenarios. To address these issues, the Pyraformer model adopted in this study significantly reduces computational overhead while enhancing the capacity to capture long-range temporal dependencies.

Since its introduction by Liu et al. (2022), the Pyraformer model has gradually been adopted in various complex forecasting scenarios owing to its high efficiency and strong generalisation capability in long-sequence modelling. For example, Dong et al. (2023) applied Pyraformer to the prediction of heavy metal contamination risk in wheat, providing effective technical support for food safety assessment and early warning system development. Tang et al. (2023) combined an improved VMD method with the Adan optimiser for electricity load forecasting, significantly enhancing prediction accuracy. Hu et al. (2023)

https://doi.org/10.5194/egusphere-2026-1715
Preprint. Discussion started: 27 March 2026

further improved model performance in multi-step forecasting of main steam flow in waste incineration by incorporating PCA. In addition, the model has been improved to better cope with abrupt variations in time series (Li and Cai, 2023), and high-precision electricity load forecasting has been achieved through a multi-module framework (Li et al., 2024b). With its high modelling efficiency, strong capability for capturing global dependencies, and advantages in uncertainty modelling, the Pyraformer model offers valuable methodological insights for seismic research. In particular, when dealing with the sparsity, abrupt variations, and strong spatiotemporal correlations inherent in seismic data, Pyraformer demonstrates considerable research and application potential.

As shown in Figure 3, the Pyraformer model consists of three main components: a Pyramid-style sparse Attention Mechanism (PAM), a Context Selection and Correlation Module (CSCM), and a prediction module. Unlike traditional full self-attention methods, the encoder progressively compresses the input time series through local dependency construction and a hierarchical pyramidal downsampling structure, thereby reducing computational complexity while enhancing the modelling of long-range temporal dependencies. The CSCM is designed to compensate for the information loss caused by downsampling. By preserving key local temporal features, it facilitates the transmission and fusion of multi-scale information. The PAM extracts temporal feature representations at multiple time scales and forms hierarchical representations through progressive aggregation. Finally, the prediction module integrates these multi-level features to generate the complete prediction sequence in a single step, thereby improving inference efficiency while maintaining prediction accuracy.

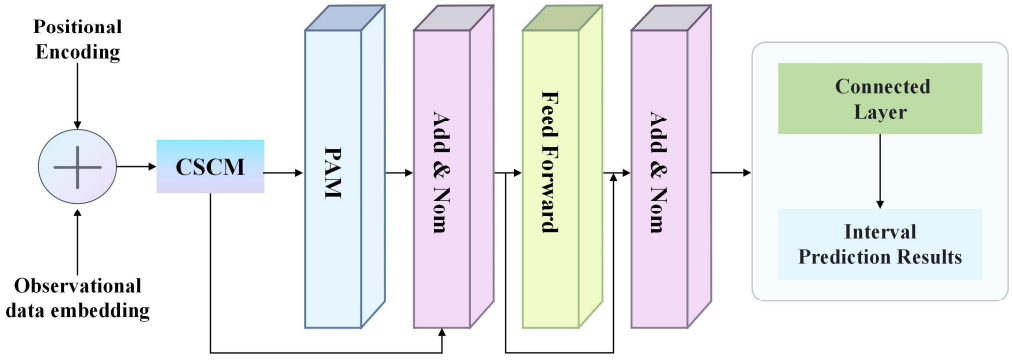

Figure 3: Pyraformer network architecture diagram.

Pyraformer replaces the fully connected self-attention architecture used in traditional Transformer models by introducing the PAM. By establishing local dependencies and combining them with a hierarchical downsampling strategy, this mechanism effectively reduces redundant connections in attention computation, thereby significantly lowering computational complexity

https://doi.org/10.5194/egusphere-2026-1715
Preprint. Discussion started: 27 March 2026

and memory overhead. While maintaining computational efficiency, it preserves the ability to model long-range dependencies. Through multi-level operations and self-attention mechanisms, the pyramid module effectively extracts and integrates local temporal features across multiple scales, thereby providing efficient and information-rich feature representations for subsequent prediction tasks.

$$\begin{cases} Attention(Q,K,V) = softmax\left(\frac{QK^T}{\sqrt{d}}\right)V \\ SparseAttention(Q,K,V) = softmax(\frac{M(QK^T)}{\sqrt{d}})V \end{cases}, \quad (6)$$

where, Q, K and V denote the input matrices of the attention mechanism; d denotes the dimension of the query vector (the input dimension); M denotes the mask function, which controls which positions can be attended to (local or skip connections).

As shown in Figure 4, from the outermost layer to the innermost layer, the red solid lines represent the longest paths required for information transmission between any two nodes; the black dashed lines denote cross-scale information interactions between different hierarchical levels; the blue solid lines represent local dependencies between nodes within the same scale; and the orange dashed lines denote the self-attention mechanism of each node.

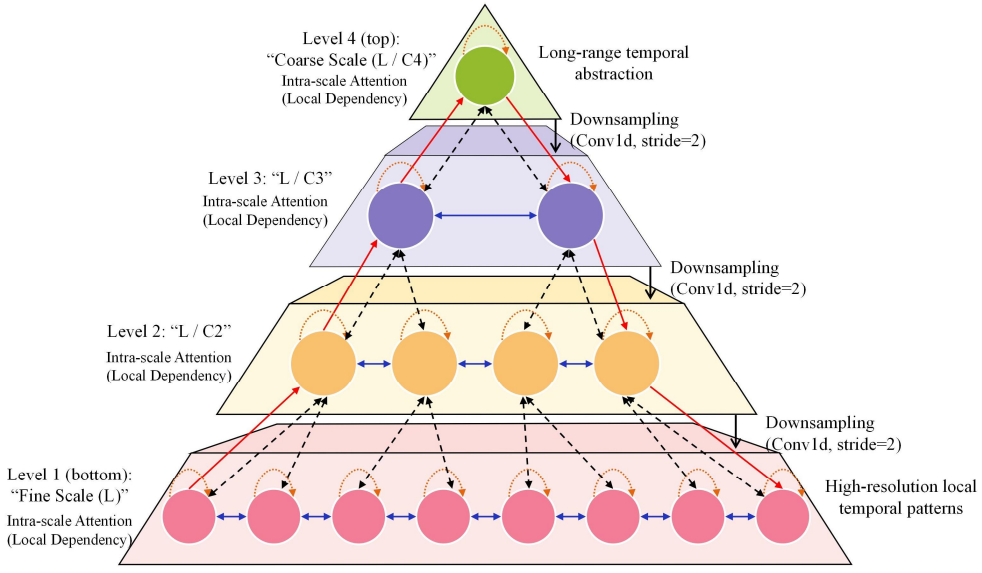

Figure 4: Schematic diagram of the pyramid-style sparse attention mechanism.

To avoid the loss of key fluctuation features and anomalous variation patterns during time-series downsampling, a CSCM is introduced before the pyramidal encoder to perform context fusion on the input data. This module employs an attention

https://doi.org/10.5194/egusphere-2026-1715
Preprint. Discussion started: 27 March 2026

mechanism to select the local temporal information from the original high-temporal-resolution sequence that is most relevant to the current downsampling node. As shown in Figure 5, the CSCM consists of a multi-layer one-dimensional convolutional structure, in which each convolutional layer is sequentially applied to the embedded input sequence along the temporal dimension, with both the kernel size and stride set to C. After the n-th convolutional operation, the length of the generated feature sequence corresponds to the scale of the node in the pyramidal multi-branch tree structure. Before being fed into the PAM, the feature sequences generated at different resolutions are concatenated by the CSCM from fine to coarse to achieve cross-scale information fusion. To reduce the number of model parameters and the computational burden, the feature dimension of each node is first compressed through a fully connected layer before the sequences enter the stacked convolutional layers; after all convolution operations are completed, the feature dimension is mapped back to the original space. In the figure, C denotes the stride, B denotes the batch size, L denotes the sequence length, and D denotes the feature dimension.

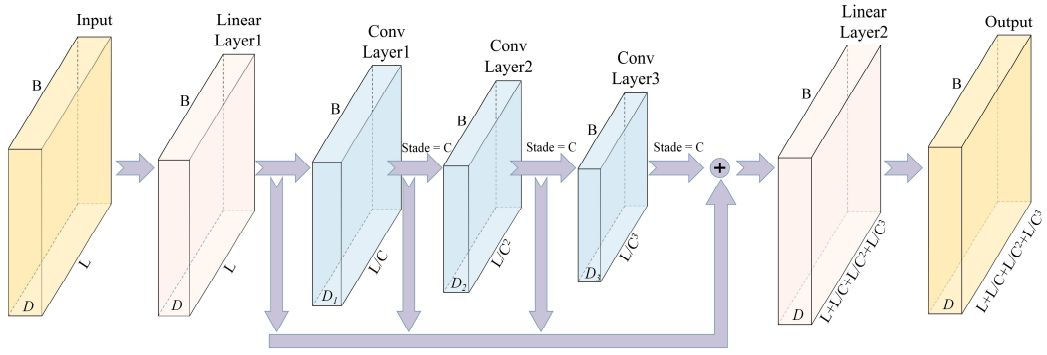

Figure 5: Block diagram of the CSCM module.

To evaluate the performance of the Pyraformer model relative to other deep learning methods in detecting anomalous features in seismic data, three benchmark models, namely the LSTM, GRU, and Transformer models, were selected for comparative experiments. These models were trained on seismic observation data using standard parameter settings. To provide a clearer quantitative comparison of model performance, a representative anomalous day, 1 March 2013, was selected as a case study. The corresponding results are presented in Figure 6 and Table 2.

https://doi.org/10.5194/egusphere-2026-1715
Preprint. Discussion started: 27 March 2026

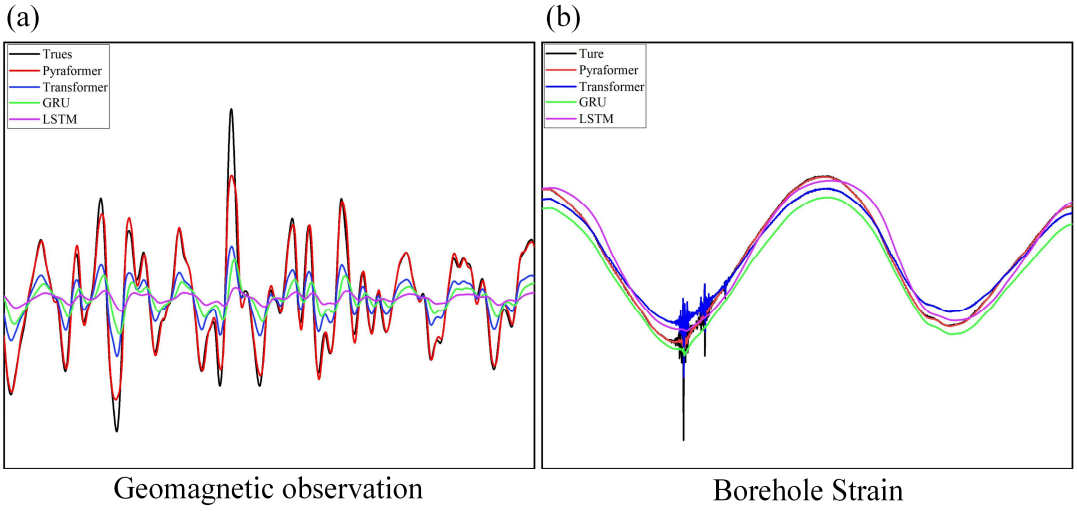

Figure 6: Comparison of model fitting results. Pyraformer achieves better fitting results than the other three models.

Data	Model	MSE	MAE	RMSE	sMAPE
Geomagnetic Observation	Pyraformer	0.0779	0.156934	0.279105	26.82%
	Transformer	0.067904	0.15063	0.260584	26.65%
	GRU	0.385825	0.441881	0.621148	98.55%
	LSTM	0.71271	0.614871	0.844221	145.27%
Borehole Strain	Pyraformer	47.278270	1.828471	6.875920	4.486 %
	Transformer	169.051957	9.563136	13.001998	21.686 %
	GRU	566.009931	22.339782	23.790963	50.917 %
	LSTM	275.533514	12.638115	16.599202	34.932 %

Table 2: Evaluation metrics for model prediction results.

The comparison of model fitting results shows that Pyraformer can reproduce the overall trends of the observed sequences for both geomagnetic observations and borehole strain data with high fidelity. Its predicted curves show strong consistency in phase, oscillatory structure, and long-term evolutionary characteristics, thereby making anomalous variations more distinguishable. In contrast, both GRU and LSTM exhibit evident amplitude deviations and phase-lag effects for both types of data, which limit their ability to effectively capture the complex temporal structures contained in the observational sequences. Although the Transformer can fit local variations relatively well during certain periods, its performance remains limited in maintaining consistency with the overall trend and preserving multi-scale structural information.

A further examination of the quantitative evaluation metrics shows that, for geomagnetic observation data, Pyraformer achieves error values (MSE, MAE, RMSE, and sMAPE) that are broadly comparable to those of the Transformer model,

https://doi.org/10.5194/egusphere-2026-1715
Preprint. Discussion started: 27 March 2026

although some metrics are slightly less favourable. This difference is closely related to the structural characteristics of the two models. Transformer-based methods emphasise point-wise alignment at individual time steps and therefore have a relative advantage in minimising local prediction errors. By contrast, Pyraformer relies on a pyramidal temporal decomposition architecture to model multi-scale temporal dependencies and global evolutionary characteristics. Consequently, its predictions are more effective in preserving smooth overall trends and structural consistency, even though this may involve a slight sacrifice in point-wise precision. In the case of borehole strain data, Pyraformer clearly outperforms the other three models across all error metrics, highlighting its particular strength in modelling time series characterised by dominant low-frequency components, pronounced trends, and strong structural background control.

Based on the combined qualitative fitting results and quantitative evaluation, the results indicate that Pyraformer effectively balances the ability to capture overall trends with structural stability in modelling multi-source seismic observation data, thereby facilitating subsequent anomaly extraction and pre-earthquake evolution analysis based on prediction residuals. Therefore, Pyraformer was selected as the unified prediction model for geomagnetic and borehole strain observation data in this study.

4 Data Analysis

All seismic observation data used in this study were provided by the Beijing Seismological Bureau. Given the occurrence of the Ms 7.0 Lushan earthquake in Sichuan on 20 April 2013, appropriate time windows were selected for different types of observational data for subsequent analysis, with the aim of systematically characterising the evolution of pre-earthquake anomalies. Specifically, geomagnetic observation data from the Chengdu, Xichang, and Muli stations covering the period from 1 January 2013 to 30 April 2013 were selected to characterise the short- to medium-term background variations of geomagnetic disturbances prior to the earthquake. Meanwhile, borehole strain data from the Kangding and Xiaomiao stations spanning 1 May 2012 to 30 April 2013 were selected to characterise the strain evolution over a longer time scale.

To effectively separate multi-scale disturbance components in geomagnetic and borehole strain observation sequences and highlight potential non-stationary features prior to earthquakes, this study employs VMD to perform frequency-domain decomposition of the data. VMD constructs a constrained variational optimisation model to decompose the original complex signal into several IMFs with finite bandwidths, with each mode corresponding to a relatively independent centre frequency in the frequency domain, thereby enabling multi-scale and non-recursive signal decomposition. In the actual decomposition process, the number of modes was preset to 5, and the resulting components were sequentially denoted as k_1 to k_5. The bandwidth constraint parameter was set to 5000, and the convergence accuracy threshold was set to e^{-7} to ensure the stability and computational accuracy of the decomposition results.

https://doi.org/10.5194/egusphere-2026-1715
Preprint. Discussion started: 27 March 2026

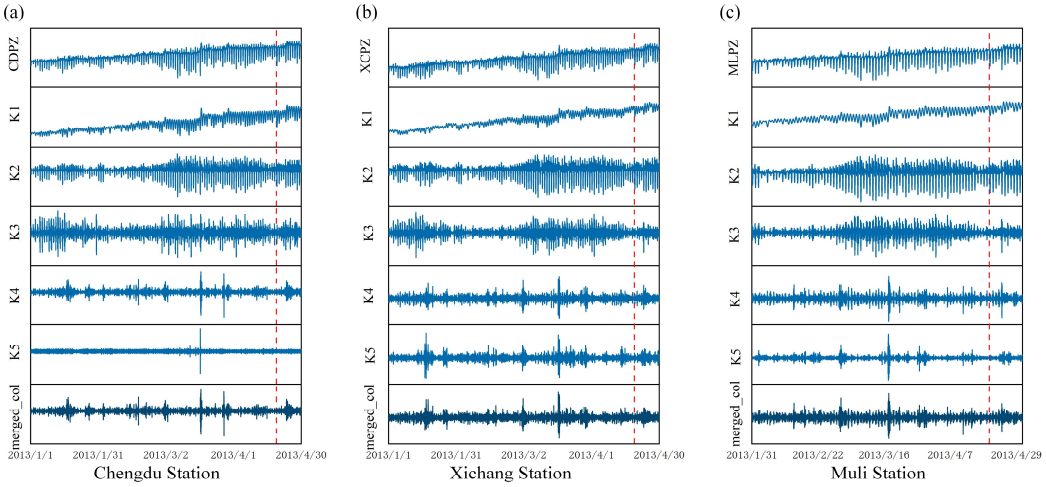

Figure 7: Decomposition of geomagnetic observation data.

Figure 7 presents the VMD decomposition results for the Chengdu, Xichang, and Muli stations during the study period of the Lushan earthquake. The decomposed modes can be characterised as follows: k_1 mainly represents the long-term background trend and very low-frequency gradual variations, k_2 and k_3 are dominated by medium-frequency oscillations and contain distinct diurnal cycles as well as certain ionospheric activity signals, in contrast, k_4 and k_5 are concentrated in the relatively high-frequency band, exhibiting small amplitudes but frequent fluctuations, and together form the high-frequency background. Further analysis indicates that the high-frequency band is more sensitive to short-period disturbances. Prior to an earthquake or under strong external disturbances, its amplitude and local energy often exhibit anomalous changes at an earlier stage. Therefore, this study adopts the reconstructed signal obtained by superimposing the two high-frequency modal components (k_4+k_5) to characterise the key high-frequency fluctuation features of the geomagnetic time series.

https://doi.org/10.5194/egusphere-2026-1715
Preprint. Discussion started: 27 March 2026

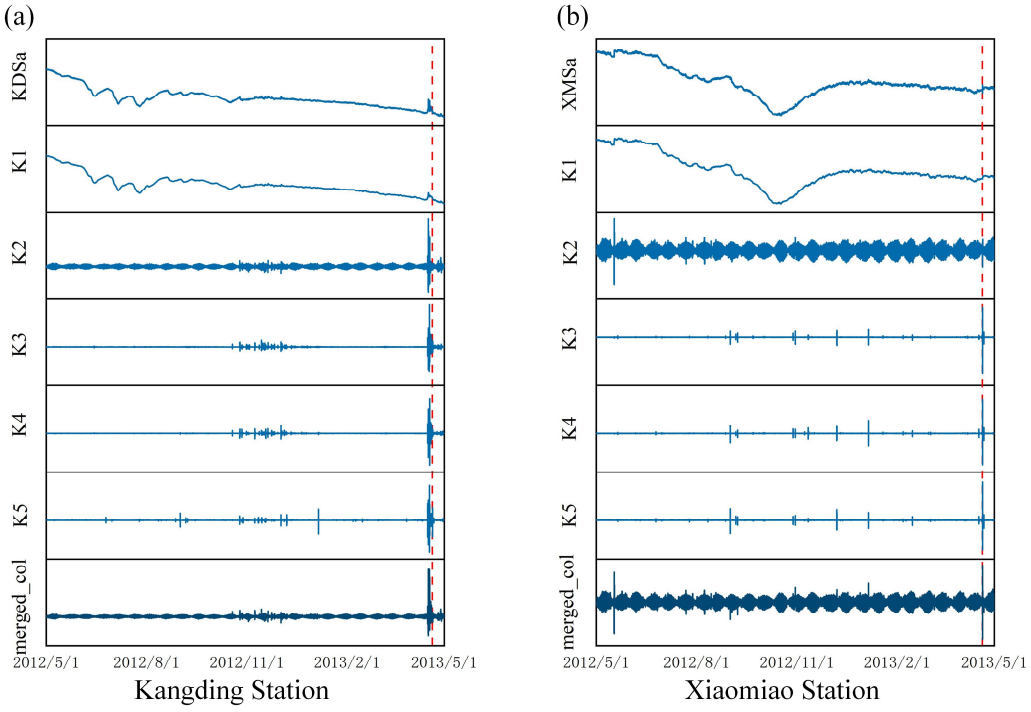

Figure 8: Breakdown of borehole strain measurement data.

Figure 8 presents the VMD decomposition results for borehole strain data from the Kangding and Xiaomiao stations during the study period of the Lushan earthquake. The decomposed modes exhibit clear differences in both temporal scale and physical significance. Specifically, k_1 represents the annual-scale trend component and primarily reflects long-term background variations, k_2 corresponds to the solid tide component and appears as pronounced periodic strain fluctuations, and k_3, k_4, and k_5 are concentrated in relatively higher-frequency bands, reflecting potential non-stationary variation characteristics. Considering the clear physical significance of solid tides in strain observations, together with the fact that high-frequency components are more sensitive to local strain perturbations prior to an earthquake, this study reconstructs the borehole strain sequence for subsequent analysis using the combined components ($k_2 + k_3 + k_4 + k_5$).

https://doi.org/10.5194/egusphere-2026-1715
Preprint. Discussion started: 27 March 2026

5 Result Analysis

5.1 Analysis of Prediction Results

This study employs an integrated VMD-Pyraformer framework to perform unified modelling and analysis of geomagnetic and borehole strain observation data, with the aim of identifying potential anomalous evolutionary characteristics prior to the 2013 Lushan M_S7.0 earthquake. By comparing model predictions for different types of observation sequences with the corresponding measured data, the model's ability to characterise normal background variations and respond to anomalous disturbances can be systematically evaluated. The following sections provide a detailed analysis of model performance, focusing on the high-frequency geomagnetic component and the reconstructed borehole strain sequence, respectively.

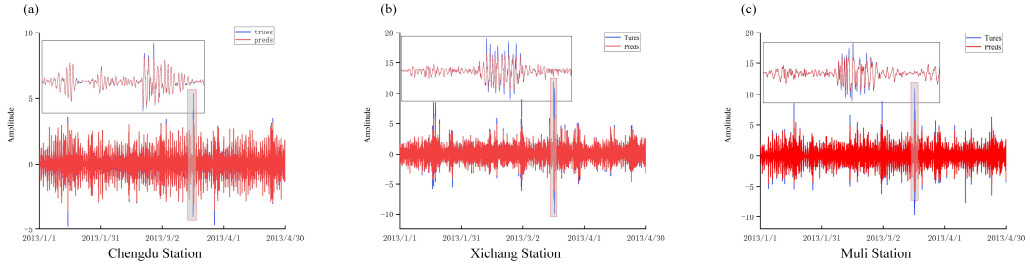

Figure 9: Detailed results of the geomagnetic data model predictions for Chengdu, Xichang and Muli.

As shown in Figure 9, for geomagnetic observations, a comprehensive analysis of data from the Chengdu, Xichang, and Muli stations indicates that the model effectively captures the background structure of the high-frequency geomagnetic component on a daily timescale. During most periods when the geomagnetic environment remained relatively stable, the predicted sequences were highly consistent with the observed data in terms of oscillation frequency, phase changes, and the positions of peaks and troughs, with overall residuals remaining small. This indicates that the model can stably learn and reproduce the normal evolutionary patterns of high-frequency geomagnetic signals. In contrast, during specific suspected disturbance periods or critical pre-earthquake intervals, the observed series exhibited sudden amplitude enhancements or abrupt shifts in extreme values, whereas the predicted results continued to follow the background pattern smoothly and failed to fully track these short-term abrupt variations, thereby producing distinct local prediction–observation discrepancies. This characteristic, namely good background fitting with significant deviations in anomalous segments, suggests that the model can effectively amplify residual signals during anomalous periods without excessively smoothing anomalous information, thus providing a reliable basis for subsequent residual-based identification of pre-earthquake disturbances.

https://doi.org/10.5194/egusphere-2026-1715
Preprint. Discussion started: 27 March 2026

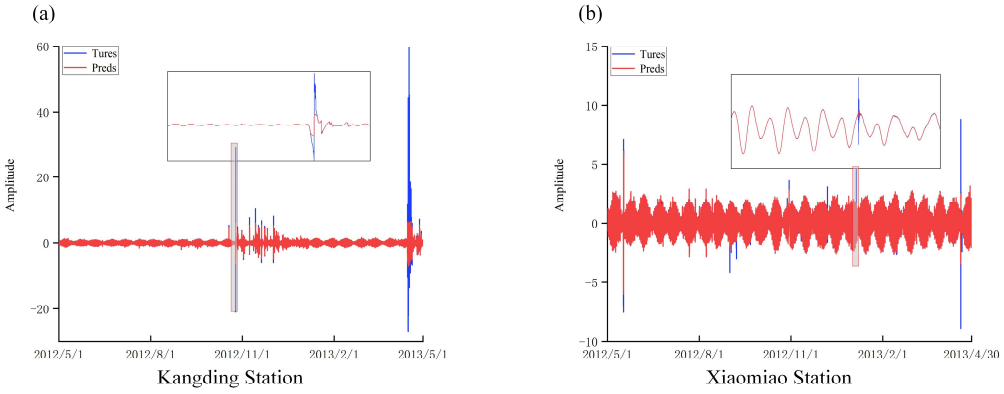

Figure 10: Detailed results of the model predictions for the strain data from the Kangding and Xiaomiao boreholes.

As shown in Figure 10, for the borehole strain observations, the model also demonstrated a strong ability to capture long-term background variations. During the vast majority of steady-state periods, the predicted curves remained highly consistent with the measured strain series in terms of overall trend, periodic fluctuations, and amplitude range, indicating that the model is capable of effectively capturing the fundamental evolutionary characteristics of borehole strain under normal tectonic loading and solid tide conditions. However, during certain critical periods, the measured strain data exhibited pronounced sudden jumps or extreme pulse-like events, with amplitudes markedly exceeding those of conventional background fluctuations. In contrast, the model predictions maintained a relatively smooth background response and did not fully track these abrupt changes synchronously, thereby producing distinct local discrepancies between predictions and observations. In particular, during phases of strong anomalies or sudden disturbances, the measured sequences showed rapid positive-to-negative transitions within a short time interval, whereas the model predictions displayed only weak responses or lagged adjustments, causing the anomalous features to be clearly highlighted in the residuals. Overall, these results indicate that the model can stably characterise both the long-term background and routine fluctuations of borehole strain while preserving key anomaly-related information in the form of significant deviations when disturbances occur, thereby providing robust support for subsequent quantitative analysis of pre-earthquake strain anomalies.

5.2 Abnormal extraction

After obtaining high-quality point prediction results for the geomagnetic and borehole strain observation sequences, this study constructs a statistical thresholding method based on prediction residuals to explicitly separate anomalous disturbances that cannot be adequately captured by the model from the normal diurnal and tectonic loading backgrounds, thereby enabling the quantitative identification of pre-earthquake anomalous signals. First, the sequence of absolute prediction residuals at each time step is defined as follows:

https://doi.org/10.5194/egusphere-2026-1715
Preprint. Discussion started: 27 March 2026

$$e_t = |y_t - \hat{y}_t|, \quad (7)$$

where, y_t denotes the observed value from geomagnetic or borehole strain observations, $\hat{y}_t$ represents the corresponding model prediction. This residual sequence reflects the component of the observed signal that is not captured by the model's fitted background component and serves as the key basis for subsequent anomaly identification.

Next, the mean of the absolute residual sequence, denoted by $\bar{e}$, is calculated, and a multiple of this value is used as the anomaly detection threshold to define a point-level anomaly criterion.:

$$e_t > k \cdot \bar{e}, \quad (8)$$

where k is an anomaly-sensitive parameter. Based on comparative experiments using multi-station geomagnetic data and borehole strain data, this study adopts $k \in [2,3]$ as the empirically optimal range. A smaller value of k tends to classify random background fluctuations as anomalies, whereas an excessively large value may obscure potential pre-seismic signals with weak amplitudes but long durations. When the residual at a given time point satisfies the above criterion, that time point is identified as anomalous. To reduce the influence of transient noise and to highlight the overall temporal characteristics of anomalous activity, this study further extends anomaly detection to the daily scale for a more comprehensive evaluation. Specifically, the number of anomalous points satisfying the above criterion within each day is counted; when the daily number of anomalous points exceeds a preset threshold, that day is defined as an anomalous day. Taking into account differences in sampling frequency and station noise levels, this study sets the daily anomaly-point threshold at approximately 40–50 for geomagnetic observation data and approximately 20–30 for borehole strain data.

Building on this, to characterise the temporal evolution of anomalous activity, this study further conducts a cumulative statistical analysis of anomalous days to construct a cumulative anomaly curve. Specifically, each day is assigned a binary label $[0, 1]$ indicating whether it is anomalous, and these values are accumulated in chronological order to form a monotonically increasing cumulative anomaly sequence. During periods of long-term background stability, the curve increases slowly with a gentle slope; as anomalous activity gradually intensifies, the slope of the cumulative curve increases markedly; and if anomalous activity tends to cluster or plateau prior to an earthquake, the curve exhibits a flattening trend in the high-value range. This indicator provides an intuitive and quantifiable means of characterising the phased evolution of geomagnetic and borehole strain anomalies, as well as their relationship with the earthquake generation process.

https://doi.org/10.5194/egusphere-2026-1715
Preprint. Discussion started: 27 March 2026

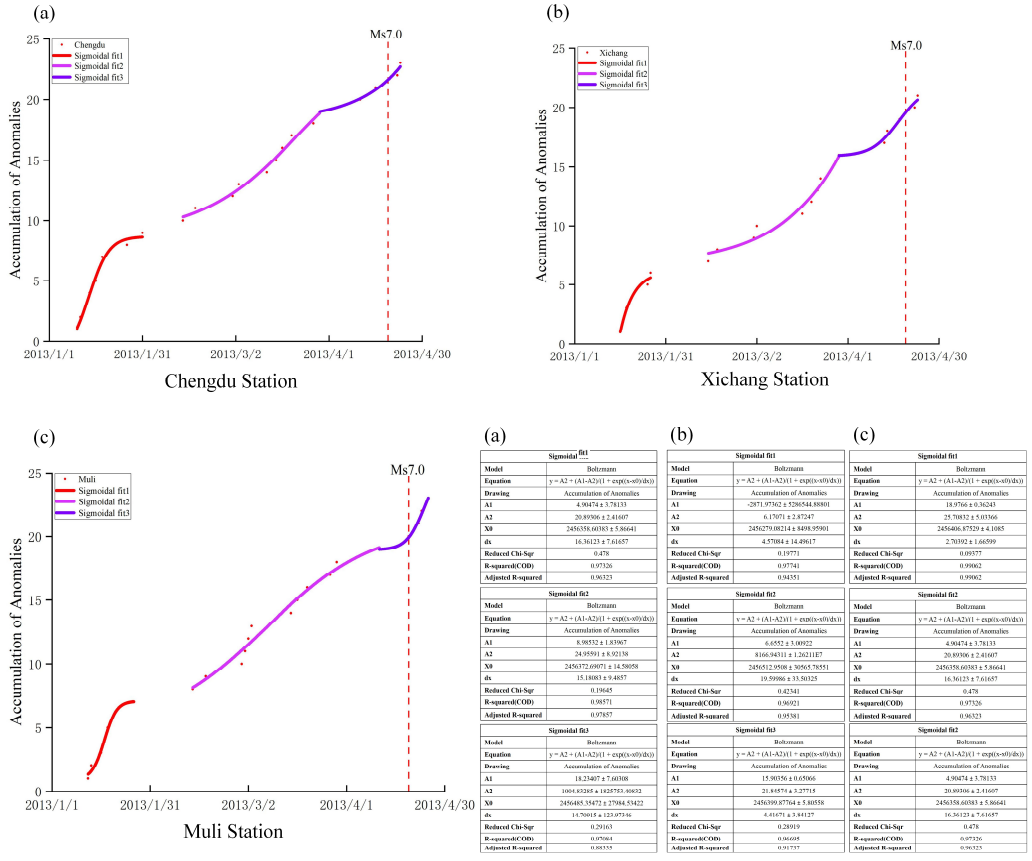

(a)

Sigmoidal fit1	
Model	Boltzmann
Equation	y = A2 + (A1-A2)/(1 + exp((x-x0)/dx))
Drawing	Accumulation of Anomalies
A1	4.90474 ± 3.78133
A2	20.89306 ± 2.41607
X0	2456358.60383 ± 5.86641
dx	16.36123 ± 7.61657
Reduced Chi-Sqr	0.478
R-squared(COD)	0.97326
Adjusted R-squared	0.96323

Sigmoidal fit2	
Model	Boltzmann
Equation	y = A2 + (A1-A2)/(1 + exp((x-x0)/dx))
Drawing	Accumulation of Anomalies
A1	8.98532 ± 1.83967
A2	24.95591 ± 8.92138
X0	2456372.69071 ± 14.58058
dx	15.18083 ± 9.4857
Reduced Chi-Sqr	0.19645
R-squared(COD)	0.98571
Adjusted R-squared	0.97857

Sigmoidal fit3	
Model	Boltzmann
Equation	y = A2 + (A1-A2)/(1 + exp((x-x0)/dx))
Drawing	Accumulation of Anomalies
A1	18.23407 ± 7.60308
A2	1004.83265 ± 1825753.40632
X0	2456485.35472 ± 27984.53422
dx	14.76015 ± 123.07356
Reduced Chi-Sqr	0.29163
R-squared(COD)	0.97661
Adjusted R-squared	0.96555

(b)

Sigmoidal fit1	
Model	Boltzmann
Equation	y = A2 + (A1-A2)/(1 + exp((x-x0)/dx))
Drawing	Accumulation of Anomalies
A1	-2871.97362 ± 5286544.88801
A2	6.17071 ± 2.87247
X0	2456279.08214 ± 8498.95901
dx	4.57084 ± 14.49617
Reduced Chi-Sqr	0.19771
R-squared(COD)	0.97741
Adjusted R-squared	0.94351

Sigmoidal fit2	
Model	Boltzmann
Equation	y = A2 + (A1-A2)/(1 + exp((x-x0)/dx))
Drawing	Accumulation of Anomalies
A1	6.6552 ± 3.00922
A2	8166.94311 ± 1.26211E7
X0	2456512.9508 ± 30565.78551
dx	19.59986 ± 33.50325
Reduced Chi-Sqr	0.42541
R-squared(COD)	0.96921
Adjusted R-squared	0.95381

Sigmoidal fit3	
Model	Boltzmann
Equation	y = A2 + (A1-A2)/(1 + exp((x-x0)/dx))
Drawing	Accumulation of Anomalies
A1	15.90356 ± 0.65066
A2	21.85574 ± 3.27715
X0	2456399.87764 ± 5.80558
dx	4.41671 ± 3.84127
Reduced Chi-Sqr	0.28919
R-squared(COD)	0.96495
Adjusted R-squared	0.91737

(c)

Sigmoidal fit1	
Model	Boltzmann
Equation	y = A2 + (A1-A2)/(1 + exp((x-x0)/dx))
Drawing	Accumulation of Anomalies
A1	18.9766 ± 0.36243
A2	25.70832 ± 5.03366
X0	2456486.87529 ± 4.1085
dx	2.70392 ± 1.66599
Reduced Chi-Sqr	0.09377
R-squared(COD)	0.99062
Adjusted R-squared	0.99062

Sigmoidal fit2	
Model	Boltzmann
Equation	y = A2 + (A1-A2)/(1 + exp((x-x0)/dx))
Drawing	Accumulation of Anomalies
A1	4.90474 ± 3.78133
A2	20.89306 ± 2.41607
X0	2456358.60383 ± 5.86641
dx	16.36123 ± 7.61657
Reduced Chi-Sqr	0.478
R-squared(COD)	0.97326
Adjusted R-squared	0.96323

Sigmoidal fit3	
Model	Boltzmann
Equation	y = A2 + (A1-A2)/(1 + exp((x-x0)/dx))
Drawing	Accumulation of Anomalies
A1	4.90474 ± 3.78133
A2	20.89306 ± 2.41607
X0	2456358.60383 ± 5.86641
dx	16.36123 ± 7.61657
Reduced Chi-Sqr	0.478
R-squared(COD)	0.97326
Adjusted R-squared	0.96323

Figure 11: Cumulative results of the number of days with geomagnetic anomalies in Chengdu, Xichang and Muli.

As shown in Figure 11, the cumulative statistical analysis of geomagnetic anomalies prior to the Lushan earthquake, combined with sigmoid-function fitting, indicates that the Chengdu, Xichang, and Muli stations all exhibited a common evolutionary pattern characterised by a transition from slow to rapid growth during the earthquake preparation stage. Inter-station differences in the onset time, growth rate, and cumulative amplitude of the anomalies reflect the spatial heterogeneity of regional tectonic stress loading and the response characteristics of the geological medium (Huang, 1994). Further analysis of the temporal evolution of geomagnetic anomalies suggests that their pre-earthquake development can be divided into three stages. The first stage began in early January, approximately 100 days before the earthquake, during which anomalous signals appeared sporadically and then temporarily stabilised by the end of the month. The second stage started in early February, when the cumulative growth rate of anomalies increased markedly and continued to intensify through the end of

https://doi.org/10.5194/egusphere-2026-1715
Preprint. Discussion started: 27 March 2026

March, corresponding to approximately 70 to 20 days before the earthquake, indicating the persistence and expansion of anomalous activity. The third stage began in early April, during which the slope of the cumulative anomaly curve increased rapidly, anomaly points became highly concentrated, and this accelerated trend persisted until the earthquake occurred, showing a distinct pre-earthquake acceleration pattern. The latter two stages of this three-stage evolutionary pattern are highly consistent with the results reported by Yu et al. (2024) for geomagnetic anomalies associated with the Lushan earthquake in terms of both variation characteristics and overall trend. This suggests that the prediction-residual-based anomaly identification method adopted in this study not only reliably reproduces the pre-earthquake characteristics reported in previous studies, but also further clarifies the continuity of anomaly development during the early stage.

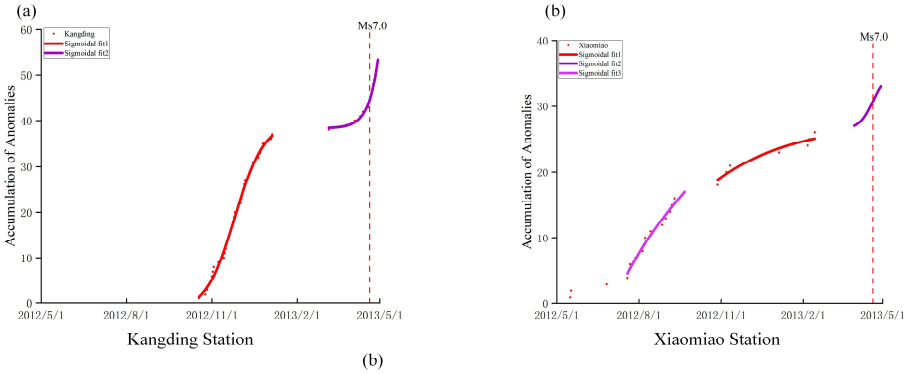

(a)

Sigmoidal fit1	
Model	Boltzmann
Equation	y = A2 + (A1-A2)/(1 + exp((x-x0)/dx))
Drawing	Accumulation of Anomalies
A1	-1.75164 ± 1.08384
A2	39.64863 ± 0.99161
X0	2456256.76679 ± 0.79251
dx	15.67879 ± 1.10634
Reduced Chi-Sqr	0.55316
R-squared(COD)	0.99567
Adjusted R-squared	0.99528

Sigmoidal fit2	
Model	Boltzmann
Equation	y = A2 + (A1-A2)/(1 + exp((x-x0)/dx))
Drawing	Accumulation of Anomalies
A1	38.33935 ± 0.48396
A2	411.71885 ± 3781.68334
X0	2456442.8397 ± 99.4651
dx	10.03638 ± 2.69847
Reduced Chi-Sqr	0.24592
R-squared(COD)	0.99132
Adjusted R-squared	0.98915

(b)

Sigmoidal fit1	
Model	Boltzmann
Equation	y = A2 + (A1-A2)/(1 + exp((x-x0)/dx))
Drawing	Accumulation of Anomalies
A1	-15095.22148 ± 1.83336E8
A2	77.46013 ± 19.79169
X0	2455596.05921 ± 1032379.81511
dx	84.6947 ± 701.12157
Reduced Chi-Sqr	0.6866
R-squared(COD)	0.94278
Adjusted R-squared	0.90845

Sigmoidal fit2	
Model	Boltzmann
Equation	y = A2 + (A1-A2)/(1 + exp((x-x0)/dx))
Drawing	Accumulation of Anomalies
A1	26.42418 ± 0.26684
A2	34.9744 ± 0.77478
X0	2456401.72997 ± 1.28002
dx	7.7206 ± 1.12101
Reduced Chi-Sqr	0.01077
R-squared(COD)	0.99885
Adjusted R-squared	0.99769

Sigmoidal fit3	
Model	Boltzmann
Equation	y = A2 + (A1-A2)/(1 + exp((x-x0)/dx))
Drawing	Accumulation of Anomalies
A1	-3836.62885 ± 3993823.81295
A2	34.75357 ± 151.88038
X0	2455538.58518 ± 133079.71046
dx	121.34471 ± 1553.97958
Reduced Chi-Sqr	0.40928
R-squared(COD)	0.98201
Adjusted R-squared	0.97661

Figure 12: Cumulative results of the number of days with abnormal strain data from the Kangding and Xiaomiao boreholes.

As shown in Figure 12, the cumulative evolution of anomalies in borehole strain observations at the Kangding and Xiaomiao stations exhibits a similar pattern, transitioning from a phase of slow accumulation to one of rapid intensification. The degree of coordination observed during this process can serve as an indicator of the regional stress state, with the evolution typically progressing through a nonlinear phase followed by a sub-instability stage (Ma and Guo, 2014). From the inter-station comparison, the anomaly extraction results at the Kangding station are highly consistent with those reported by Chi et al. (2023) for the Lushan earthquake, with the accelerated anomaly phase in both cases beginning in November 2012. The anomaly extraction results at the Xiaomiao station are likewise broadly consistent with those reported by Li et al. (2024a), both showing a distinct three-stage evolutionary pattern. It is noteworthy that anomalies at the Xiaomiao station appeared earlier than those at the Kangding station. This observation is consistent with the views of King et al. (1994) and Stein (1999), who emphasised that the spatiotemporal distribution of pre-earthquake anomalies is not simply controlled by the

https://doi.org/10.5194/egusphere-2026-1715
Preprint. Discussion started: 27 March 2026

distance between a station and the future epicentre, but is more strongly influenced by fault geometry, fault segmentation, and stress transfer processes. Further temporal comparison indicates that anomalous signals began to appear at both stations approximately six months before the earthquake, starting in November 2012 and continuing to accumulate until early March 2013. Thereafter, both the number of anomalous days and the cumulative anomaly amplitude increased rapidly, reaching a peak during the immediate pre-seismic stage. These results indicate that the prediction-residual-based anomaly identification method can effectively extract anomalous signals from borehole strain observations that are closely associated with the evolution of pre-seismic tectonic stress, while also reliably reproducing the typical pre-earthquake strain anomaly characteristics reported in previous studies. This further validates the reliability and applicability of the proposed method for borehole strain precursor analysis.

An analysis of the cumulative evolution of geomagnetic and borehole strain data reveals that these two physical quantities exhibit a clear temporal correspondence and coupling relationship during the pre-earthquake stage. Specifically, borehole strain anomalies begin to accumulate earlier at some stations, whereas geomagnetic anomalies subsequently undergo accelerated accumulation along adjacent fault segments. Overall, this pattern is characterised by strain anomalies preceding geomagnetic anomalies, expansion from local to regional scales, and stage-wise accelerated accumulation. This coupling is reflected not only in the sequence of occurrence, with strain anomalies appearing before geomagnetic anomalies, but also in their amplitude and rate-of-change characteristics. In particular, the rapid growth phase of cumulative borehole strain anomalies is typically separated by several days from the corresponding rapid growth phase of geomagnetic anomalies, suggesting that localised stress concentration may be transmitted to the local magnetic field through coupling within the medium.

In terms of spatial distribution, strain and geomagnetic anomalies at different fault segments and stations exhibit a pattern of progressive expansion. Initially, local strain anomalies are concentrated in active fault segments and then spread to surrounding stations, accompanied by the cumulative development of geomagnetic anomalies. This pattern reflects the spatial propagation of the lithospheric stress-strain field as expressed in electromagnetic field responses. Further analysis suggests that strain accumulation among different fault segments exhibits a degree of coordination, while geomagnetic anomalies at adjacent stations also show synchronous enhancement. Such synchrony and cross-field coordination indicate strong coupling between local stress-strain processes and geomagnetic responses during the earthquake preparation stage.

From the perspective of potential physical mechanisms, the observed coupling between borehole strain and geomagnetic anomalies can be attributed to microfracture activity and pressure changes induced by local stress accumulation, which subsequently affect the geomagnetic field through the electrical conductivity of the medium and stress–magnetic coupling, thereby generating observable cumulative anomalies (Gao et al., 2025). The time lag observed between borehole strain and geomagnetic anomalies is explained by electrokinetic effects in the porous fault-zone medium. Variations in high pore pressure within the fault zone drive fluid flow, inducing significant electromagnetic anomalies (Fenoglio et al., 1995) Subsurface fluids percolate through the porous rock medium, and the relative motion at the solid–liquid interface generates streaming currents, which in turn excite geomagnetic anomalies (Ren et al., 2016).

https://doi.org/10.5194/egusphere-2026-1715
Preprint. Discussion started: 27 March 2026

During the late stage of the Lushan earthquake preparation, local stress concentration along the Longmen Shan Fault Zone induced microfracturing and volumetric expansion of the rock, which were instantaneously captured by borehole strainmeters. The diffusion and migration of fluids through the complex porous fault-zone medium require time, depending on rock permeability and pore-pressure gradients, which directly accounts for the observed lag of geomagnetic anomalies relative to the earlier strain anomalies by several days to weeks. Stress–strain accumulation first triggers a local geomagnetic response, while the spatial expansion and synchronous enhancement of anomalies reflect stress propagation along fault segments and the influence of the medium on electromagnetic responses at neighbouring stations (Stein, 1999). Therefore, the relationship between borehole strain and geomagnetic anomalies is not limited to simple temporal or amplitude correspondence, but represents a cross-scale coupling mechanism extending from local stress accumulation to regional electromagnetic responses. This mechanism provides a reliable basis for multi-station, multi-parameter joint monitoring and further suggests that integrating cumulative anomalies from different physical quantities with their coupling characteristics can substantially enhance the stability and interpretability of short-term earthquake anomaly identification.

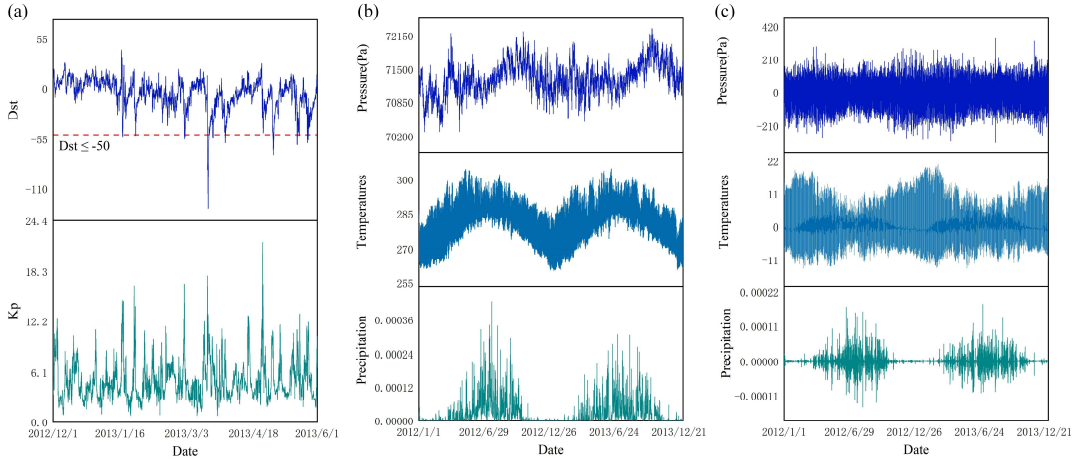

Figure 13: Environmental factors.

To ensure that the identification of pre-earthquake geomagnetic and borehole strain anomalies was not affected by external environmental disturbances, this study systematically analysed space weather and meteorological factors during the observation period. As shown in Figure 13, for the geomagnetic data, the Dst and Kp indices were examined on a daily basis over the Lushan earthquake study period (1 January-30 April 2013), and potential geomagnetic storm events were screened according to the international geomagnetic storm criteria ($Dst \leq -50nT, Kp \geq 5$). The results show that the Dst index remained mainly within the normal range of -20 to -40 nT, with only short-lived low-value excursions on 20 February, 17 March, and 13 April (approximately one week before the earthquake); none of these events reached the threshold for a moderate geomagnetic storm. During the same period, several isolated peaks of the Kp index approached 5, but their

https://doi.org/10.5194/egusphere-2026-1715
Preprint. Discussion started: 27 March 2026

duration was extremely short and they did not constitute typical geomagnetic storm events. These results suggest that the amplification of high-frequency geomagnetic fluctuations and the abrupt residual variations were primarily associated with local seismogenic processes rather than global space weather disturbances. For the strain observations, first-order differencing was applied to the daily regional mean values of air pressure, temperature, and precipitation over the two-year period from 2012 to 2013 in order to suppress periodic components. The results indicate that these meteorological factors did not exhibit significant anomalous fluctuations or structural changes prior to the earthquake. Overall, the comprehensive analysis suggests that external environmental factors exerted only limited influence on the geomagnetic and borehole strain anomaly signals. This further supports the interpretation that the observed anomalies were related to the earthquake preparation process, thereby providing a reliable basis for subsequent anomaly identification and earthquake preparation analysis.

5.3 Analysis of Anomalies

In recent years, numerous studies have systematically investigated the pre-earthquake anomalies associated with the 2013 Ms 7.0 Lushan earthquake in Sichuan from multiple observational perspectives. These studies have drawn upon multi-source observational data, including underground fluids, surface thermal conditions, and ionospheric parameters, thereby providing valuable insights into the earthquake preparation process and the associated multi-physical-field responses.

With respect to subsurface fluid observations, Ye et al.(2015) analysed long-term radon concentration and water-level data from stations surrounding the epicentres of two major earthquakes along the Longmen Shan Fault Zone. Their results showed a clear positive correlation between radon concentration changes and water-level fluctuations prior to the earthquakes, indicating that significant adjustments occurred in the subsurface medium during the stress-loading stage. Based on remote sensing data, Zhang et al.(2016) investigated variations in Land Surface Temperature (LST) near the Longmen Shan Fault Zone, and the results indicated a certain degree of anomalous enhancement in LST during the pre-earthquake stage. Ma et al.(2015) analysed air-temperature variations in the vicinity of the seismic zone and found that the evolutionary characteristics of these temperature variations resembled the stress-induced rock fracturing process, suggesting that temperature changes may respond to pre-earthquake stress accumulation. In addition, Zhang et al.(2025b) examined Latent Heat Flux (LHF) variations before and after the earthquake and found that LHF increased significantly in the months preceding the event, with a spatial correlation with fault-zone activity, indicating its potential as a precursor indicator. With respect to the space-based electromagnetic environment, Shi et al.(2019) used ionospheric Total Electron Content (TEC) derived from GPS observations and, after excluding the influence of solar activity and lower-atmospheric thermal effects, identified a distinct local ionospheric anomaly near the epicentre approximately one month before the Lushan earthquake.

https://doi.org/10.5194/egusphere-2026-1715
Preprint. Discussion started: 27 March 2026

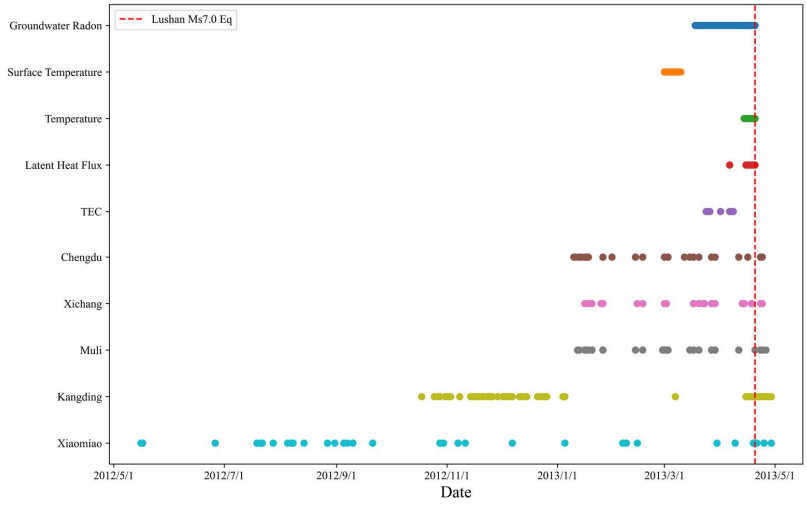

Figure 14: Anomaly Duration Statistics Chart.

As shown in the figure 14, the time-series analysis of anomalies indicates that the identified pre-earthquake anomalies extend across multiple geophysical layers, ranging from the deep crust to near-Earth space. These include deep responses such as borehole strain and groundwater radon, near-surface indicators such as land surface temperature, and upper-atmospheric observations such as ionospheric TEC. Taken together, these anomalies exhibit clear characteristics of synergistic responses across multiple scales and physical fields. The geomagnetic and borehole strain data used in this study show good consistency with the temporal evolution of the above-mentioned multi-source anomalies. By integrating the temporal evolution patterns of these anomalous responses with a comparative analysis of multi-source observational results, it can be inferred that the anomalous signals identified in the geomagnetic and borehole strain data may be related to the preparation and development process of this earthquake within the study area.

6 Conclusion

In summary, the proposed VMD-Pyraformer framework shows strong effectiveness and stability in identifying pre-earthquake anomalies from geomagnetic and borehole strain observations. It effectively separates background evolution from anomalous disturbances and reveals a clear coupling relationship between the two datasets, with borehole strain anomalies generally preceding geomagnetic anomalies. These results indicate that borehole strain may capture the earlier response of local stress accumulation, whereas geomagnetic anomalies may reflect the subsequent electromagnetic response. Therefore, the proposed framework provides an effective tool for both reliable anomaly identification and the analysis of multi-physical-field coupling during earthquake preparation.

https://doi.org/10.5194/egusphere-2026-1715
Preprint. Discussion started: 27 March 2026

535

Data availability. Data supporting the findings of this study are available from the China Earthquake Networks Center. However, restrictions apply to the availability of these data, which were used under license for the current study and are thus not publicly available. Data are, however, available from the corresponding author (email: chicqhainnu@gmail.com) upon reasonable request and with permission from the China Earthquake Networks Center.

540

Author Contributions. Conceptualization, JZ, CC and DZ. Data curation, JZ, CC and MS. Formal analysis, JZ, CC, and CQ. Investigation, JZ, CC and SD. Methodology, CC. Resources, CC. Software, JZ, MS and YD. Supervision, CC. Validation, JZ, CC. Writing – original draft, CC and JZ. Writing – review & editing, JZ, CC and DZ.

545 *Competing interests.* The authors declare that they have no conflict of interest.

Disclaimer. Publisher's note: Copernicus Publications remains neutral with regard to jurisdictional claims made in the text, published maps, institutional affiliations, or any other geographical representation in this paper. While Copernicus Publications makes every effort to include appropriate place names, the final responsibility lies with the authors.

550

Acknowledgments. The authors would like to thank Zehua Qiu, Lei Tang, and Dehe Yang from the China Earthquake Administration for their essential help in accessing the website and downloading the strain data. The authors are also grateful to Giovanni for the meteorological data (https://giovanni.gsfc.nasa.gov/giovanni, last access: May 2025). The authors are also acknowledgement for the data support from " China Earthquake Networks Center, National Earthquake Data Center. 555 (https://data.earthquake.cn)".

Financial support. This work was supported by the Project supported by the Education Department of Hainan Province，project number：Hnky2026ZD-4.

560

565

https://doi.org/10.5194/egusphere-2026-1715
Preprint. Discussion started: 27 March 2026

References

Abduallah, Y., Wang, J. T., Xu, C., and Wang, H.: A transformer-based framework for geomagnetic activity prediction, International Symposium on Methodologies for Intelligent Systems, 325-335, https://dor.org/10.1007/978-3-031-16564-1_31,

Akhoondzadeh, M.: Decision Tree, Bagging and Random Forest methods detect TEC seismo-ionospheric anomalies around the time of the Chile,(Mw= 8.8) earthquake of 27 February 2010, Advances in Space Research, 57, 2464-2469, 2016,https://doi.org/10.1016/j.asr.2016.03.035

Akinaga, Y., Hayakawa, M., Liu, J., Yumoto, K., and Hattori, K.: A precursory ULF signature for the Chi-Chi earthquake in Taiwan, Natural Hazards and Earth System Sciences, 1, 33-36, 2001,https://doi.org/10.5194/nhess-1-33-2001

Asim, K., Martínez-Álvarez, F., Basit, A., and Iqbal, T.: Earthquake magnitude prediction in Hindukush region using machine learning techniques, Natural Hazards, 85, 471-486, 2017,https://doi.org/10.1007/s11069-016-2579-3

Barbour, A. J. and Agnew, D. C.: Detection of seismic signals using seismometers and strainmeters, Bulletin of the Seismological Society of America, 102, 2484-2490, 2012,https://doi.org/10.1785/0120110298

Chen, G., Li, Y., Zhang, Y., and Wu, J.: Earthquake induced a chain disasters, Earthquake research and analysis—Statistical studies, observations and planning. InTech—Open Access Publisher, 383-416, 2012,https://doi.org/10.1029/2018RG000626

Chi, C.: Research on Drilling Strain Precursor Observation Data Analysis and Anomaly Extraction, Changchun: Jilin University: 81–82, 2020, https://dor.org/10.27162/d.cnki.gjlin.2020.000174

Chi, C., Li, C., Han, Y., Yu, Z., Li, X., and Zhang, D.: Pre-earthquake anomaly extraction from borehole strain data based on machine learning, Scientific Reports, 13, 20095, 2023,https://doi.org/10.1038/s41598-023-47387-z

Chi, C., Zhu, K., Yu, Z., Fan, M., Li, K., and Sun, H.: Detecting earthquake-related borehole strain data anomalies with variational mode decomposition and principal component analysis: A case study of the Wenchuan earthquake, IEEE Access, 7, 157997-158006, 2019,https://doi.org/10.1109/ACCESS.2019.2950011

Chi, S.: Anomalous strain recorded by volumetric drilling strain gauges prior to the Wenchuan and Lushan earthquakes, Science & Technology Review, 2013,https://doi.org/10.12677/AG.2017.72022

Cui, Q.: Research on Geomagnetic Data Reconstruction Techniques, Master's degree, Nanjing Normal University, 2021, https://dor.org/10.27245/d.cnki.gnjsu.2021.000970

De Santis, A., Marchetti, D., Pavón-Carrasco, F., Cianchini, G., Perrone, L., Abbattista, C., Alfonsi, L., Amoruso, L., Campuzano, S., and Carbone, M.: Precursory worldwide signatures of earthquake occurrences on Swarm satellite data, Sci. Rep., 9, 20287 , 2019, https://dor.org/10.1038/s41598-019-56599-1.

Dobrovolsky, I., Zubkov, S., and Miachkin, V.: Estimation of the size of earthquake preparation zones, Pure and applied geophysics, 117, 1025-1044, 1979,https://doi.org/10.1007/BF00876083

Dong, W., Hu, T., Zhang, Q., Deng, F., Wang, M., Kong, J., and Dai, Y.: Prediction of food safety risk level of wheat in china based on pyraformer neural network model for heavy metal contamination, Foods, 12, 1843, 2023, https://doi.org/10.3390/foods12091843

Dragomiretskiy, K. and Zosso, D.: Variational mode decomposition, IEEE transactions on signal processing, 62, 531-544, 2013,https://doi.org/10.1109/TSP.2013.2288675

Fan, J., Tang, L., Wang, Y., Li, Y., and Liu, G.: Joint Analysis of Regional Strain Variations Based on Borehole Strainmeter and Global Navigation Satellite System Observations, Sensors & Materials, 34, 2022,https://doi.org/10.18494/SAM4198

Fang, L., Wu, J., Wang, W., Du, W., Su, J., Wang, C., Yang, T., and Cai, Y.: Aftershock observation and analysis of the 2013 M S 7.0 Lushan earthquake, Seismological Research Letters, 86, 1135-1142, 2015,https://doi.org/10.1785/0220140186

Fenoglio, M. A., Johnston, M. J. S., and Byerlee, J. D.: Magnetic and electric fields associated with changes in high pore pressure in fault zones : Application to the Loma Prieta ULF emissions, Journal of Geophysical Research, 100, 12951-12958, 1995,https://doi.org/10.1029/95JB00076

Gao, Y., Zhao, J., Zhou, G., Chen, C. H., Sun, Y. y., Zhang, X., Li, Y., Yao, C., Meng, Z., and Bai, X.: Electromagnetic Fields Generated by an Earthquake Due to the Piezomagnetic Effect, Journal of Geophysical Research: Solid Earth, 130, e2025JB031181, 2025,https://doi.org/10.1029/2025JB031181

Gladwin, M. T.: High-precision multicomponent borehole deformation monitoring, Review of Scientific Instruments, 55, 2011-2016, 1984,https://doi.org/10.1063/1.1137704

https://doi.org/10.5194/egusphere-2026-1715
Preprint. Discussion started: 27 March 2026

Gladwin, M. T. and Hart, R.: Design parameters for borehole strain instrumentation, pure and applied geophysics, 123, 59-80, 1985,https://doi.org/10.1007/BF00877049

Gokhberg, M., Morgounov, V., Yoshino, T., and Tomizawa, I.: Experimental measurement of electromagnetic emissions possibly related to earthquakes in Japan, Journal of Geophysical Research: Solid Earth, 87, 7824-7828, 1982,https://doi.org/10.1029/JB087iB09p07824

Han, P., Hattori, K., Hirokawa, M., Zhuang, J., Chen, C. H., Febriani, F., Yamaguchi, H., Yoshino, C., Liu, J. Y., and Yoshida, S.: Statistical analysis of ULF seismomagnetic phenomena at Kakioka, Japan, during 2001–2010, Journal of Geophysical Research: Space Physics, 119, 4998-5011, 2014,https://doi.org/10.1002/2014JA019789

Hayakawa, M. and Hobara, Y.: Integrated analysis of multi-parameter precursors to the Fukushima offshore earthquake (Mj= 7.3) on 13 February 2021 and lithosphere–atmosphere–ionosphere coupling channels, Atmosphere, 15, 1015, 2024,https://doi.org/10.3390/atmos15081015

Heinecke, W.: Fluxgate magnetometer with time coded output signal of the sensor, IEEE Transactions on Instrumentation and Measurement, 27, 402-405, 2007,https://doi.org/10.1109/TIM.1978.4314723

Hou, Z., An, Z., Fan, Y., Fu, A., Tan, D., and Wei, L.: Retrospective Analysis of Electric Field Anomalies Before the 6.4 Magnitude Earthquake in Yangbi County, Yunnan, CHINA EARTHQUAKE ENGINEERING JOURNAL, 43, 807-817, 2021,https://doi.org/10.3969/j.issn.1000-0844.2021.04.807.

Hu, X., Wang, W., Tang, J., and Liu, M.: Multi-Step Ahead Prediction of Main Steam Flow Using PCA and Pyraformer in MSWI Process, 2023 35th Chinese Control and Decision Conference (CCDC), 372-376, https://dor.org/10.1109/CCDC58219.2023.10326878

Huang, Q.: Direction speciality of fault network and its self-organization evolution, Crustal Deformation and Earthquake, 14, 24-28, 1994,https://doi.org/.https://kns.cnki.net/kcms2/article/abstract?v=W-y7fKBVJCx8URMVm50LFevdJJc-EyCjQGeN9Cso4MrD-5qN7X4XSlCXk1cA5mPnSY9NkffsVFjBegZ4C2Vva1QmLciFIcOtz5sCG-LbzlZ-eZPEpXIDtBaOlK6pFwgL4_NVUHUj7qOFCrzlhptHllnVDIUkBkCz&uniplatform=NZKPT&language=CHS

Huang, Y., Shi, W., Zhu, K. a., Qiu, H., Lu, Y., Liu, G., and Zhang, G.: A pre-seismic anomaly detection approach based on graph attention isomorphism network, Measurement Science and Technology, 34, 125113, 2023,https://doi.org/10.1088/1361-6501/acefeb

King, G. C., Stein, R. S., and Lin, J.: Static stress changes and the triggering of earthquakes, Bulletin of the Seismological Society of America, 84, 935-953, 1994,https://doi.org/10.1785/BSSA0840030935

Lains, M. A. P.: A magnetometer instrument for attitude determination in a nanosatellite, Master's thesis, Department of Physics, University of Oslo, 2011.
https://nva.sikt.no/filter?query=A+magnetometer+instrument+for+attitude+determination+in+a+nanosatellite

Li, C., Qin, C., Zhang, J., Duan, Y., and Chi, C.: Analysis of borehole strain anomalies before the 2017 Jiuzhaigou M s 7.0 earthquake based on a graph neural network, Natural Hazards and Earth System Sciences, 25, 231-245, 2025,https://doi.org/10.5194/nhess-25-231-2025

Li, C., Duan, Y., Han, Y., Yu, Z., Chi, C., and Zhang, D.: Extraction of pre-earthquake anomalies from borehole strain data using Graph WaveNet: a case study of the 2013 Lushan earthquake in China, Solid Earth, 15, 877-893, 2024a,https://doi.org/10.5194/se-15-877-2024

LI, G. and CAI, W.: PHOTOVOLTAIC POWER PREDICTION BASED ON IMPROVED PYRAFORMER, 2023,https://doi.org/.https://www.scientificbulletin.upb.ro/static/pdfs/rez02d_665361.pdf

Li, X., Ai, Q., and Xu, M.: RUL Prediction of Lithium-ion Batteries Based on TimeGAN-Pyraformer-BiLSTM, Engineering Letters, 32, 2024b,https://doi.org/.https://www.engineeringletters.com/issues_v32/issue_8/EL_32_8_14.pdf

Liu, L.: Exploring the characteristics and harms of earthquake disasters and measures for earthquake prevention and reduction., Disaster Reduction in China, 54-55, 2024,https://doi.org/.https://kns.cnki.net/kcms2/article/abstract?v=tMRSZR5ycIvm3bDW7fPZUqOViRefbXofzjK858DWv8wfms5DX-ahAq0AuU7jpsbdz4W_TxKqbueTQ6YXkHLyKRSzh9VGhiPV3mjKoGXlAKTDj3k1Urlh-V_AgbsYMN35kFsplOqP0i1ggTjEF5spfVp7VHyrPekTC-rjFWPpmgr-Q3sHamduCGHm5nNf-K6cbn_VbqQPYgE=&uniplatform=NZKPT&language=CHS

Liu, S., Yu, H., Liao, C., Li, J., Lin, W., Liu, A. X., and Dustdar, S.: Pyraformer: Low-complexity pyramidal attention for long-range time series modeling and forecasting, # PLACEHOLDER_PARENT_METADATA_VALUE#, https://dor.org/10.34726/2945

https://doi.org/10.5194/egusphere-2026-1715
Preprint. Discussion started: 27 March 2026

Ma, J. and Guo, Y.: Accelerated synergism prior to fault instability: Evidence from laboratory experiments and an earthquake case, Seismology and Geology, 36, 547-561, 2014,https://doi.org/10.3969/j.issn.0253-4967.2014.03.001

Ma, J., Deng, Y., Li, X., Guo, R., Zhou, H., and Li, M.: Recent advances in machine learning-enhanced joint inversion of seismic and electromagnetic data, Surveys in Geophysics, 46, 197-225, 2025,https://doi.org/10.1007/s10712-024-09867-3

Ma, W., Kong, X., Kang, C., Zhong, X., Wu, H., Zhan, X., and Joshi, M.: Research on the changes of the tidal force and the air temperature in the atmosphere of Lushan (China) Ms7. 0 earthquake, Thermal Science, 19, 487-493, 2015,https://doi.org/10.2298/tsci150403148m

Ouzounov, D., Liu, D., Chunli, K., Cervone, G., Kafatos, M., and Taylor, P.: Outgoing long wave radiation variability from IR satellite data prior to major earthquakes, Tectonophysics, 431, 211-220, 2007,https://doi.org/10.1016/j.tecto.2006.05.042

Qiu, Z., Kan, B., and Tang, L.: Conversion and Application of Four-Component Borehole Strain Observation Data, EARTH QUAKE, 29, 83-89, 2009,https://doi.org/10.3969/j.issn.1000-3274.2009.04.009.https://kns.cnki.net/kcms2/article/abstract?v=yqBhao7Q9gyicHb-rWaMDZWrMxtIuh4PoSpWEaxojXx-eV1zDitFG_ZxKkP6BAqqtHt2_iu_erN6sOdXD3MD0tiB7a5bBTCygow7GeBWtdhgjhocQOpFb40Z7SbXLZWRiDWj8xp4ji2un1qS1i3nidkRRjvhrNQT8IwPwfTrQtQrIBiwQYBCQg==&uniplatform=NZKPT&language=CHShttps://kns.cnki.net/kcms2/article/abstract?v=yqBhao7Q9gyicHb-rWaMDZWrMxtIuh4PoSpWEaxojXx-eV1zDitFG_ZxKkP6BAqqtHt2_iu_erN6sOdXD3MD0tiB7a5bBTCygow7GeBWtdhgjhocQOpFb40Z7SbXLZWRiDWj8xp4ji2un1qS1i3nidkRRjvhrNQT8IwPwfTrQtQrIBiwQYBCQg==&uniplatform=NZKPT&language=CHS

Qiu, Z., Zhang, B., Huang, X., and Ge, L.: On the cause of ground stress tensile pulses observed before the 1976 Tangshan earthquake, Bulletin of the Seismological Society of America, 88, 989-994, 1998,https://doi.org/10.1785/BSSA0880040989

Qiu, Z., Chi, S., Wang, Z., Carpenter, S., Tang, L., Guo, Y., and Yang, G.: The strain seismograms of P-and S-waves of a local event recorded by four-gauge borehole strainmeter, Earthquake Science, 28, 209-214, 2015,https://doi.org/10.1007/s11589-015-0120-5

Rabie, E., Hafez, A. G., Saad, O. M., El-Sayed, A.-H. M., Abdelrahman, K., and Al-Otaibi, N.: Geomagnetic micro-pulsation automatic detection via deep leaning approach guided with discrete wavelet transform, Journal of King Saud University-Science, 33, 101263, 2021,https://doi.org/10.1016/j.jksus.2020.101263

Ren, H., Huang, Q., and Chen, X.: Numerical simulation of seismo-electromagnetic fields associated with a fault in a porous medium, Geophysical Journal International, 206, 205-220, 2016,https://doi.org/10.1093/gji/ggw144.https://doi.org/10.1093/gji/ggw144

Shi, K., Liu, X., Guo, J., Liu, L., You, X., and Wang, F.: Pre-earthquake and coseismic ionosphere disturbances of the Mw 6.6 Lushan earthquake on 20 April 2013 monitored by CMONOC, Atmosphere, 10, 216, 2019,https://doi.org/10.3390/atmos10040216

Sikder, I. U. and Munakata, T.: Application of rough set and decision tree for characterization of premonitory factors of low seismic activity, Expert Systems with Applications, 36, 102-110, 2009,https://doi.org/10.1016/j.eswa.2007.09.032

Stein, R. S.: The role of stress transfer in earthquake occurrence, Nature, 402, 605-609, 1999,https://doi.org/10.1038/45144

Su, K.: Analysis of Surface Strain and Shear Strain from Four Component Borehole Strain Observation Data, Earthquake Research in Shanxi, 1, 30-35, 2019,https://doi.org/.https://kns.cnki.net/kcms2/article/abstract?v=yqBhao7Q9gyXQ7WXf70T6jzVrk5hqgREejrJAjSOpwtXoZDOk_iNECYYDMcQMvlQN3NoesnuSxD9sdz093ABtVD19tJfT8KKrptdYxI6uoCbajK6kg3fQ8SSCJWYjvRChaBbuAG5H80UB1IhNsCzXOR9jXdbU-JuyEL6Zdvw7Di88SWQPuTDqTUSnHyLhikX&uniplatform=NZKPT&language=CHS

Tang, L. and Jin, Y.: Analysis of Co-seismic Strain Steps Recorded by Four-Component Strain Meters in Sichuan-Yunnan Region, Technology for Earthquake Disaster Prevention, 2013,https://doi.org/.https://kns.cnki.net/kcms2/article/abstract?v=W-y7fKBVJCz_i-DRn6p_uLp-DpLIbsPmNGfBtcdfn_IWGK-9ViA4g_tPL3zar5UHoIAQ_91Ni5gvGGTWssVhWSmqanhrOQUYKq_jkI18whmXEiC8-jOsHTTTwbq0BnreUA-1Vh9lBKqmrtrt2KmJyV5TOeGAhccnQfYmG7xfkto=&uniplatform=NZKPT&language=CHS

Tang, Y. and Cai, H.: Short-term power load forecasting based on vmd-pyraformer-adan, IEEE Access, 11, 61958-61967, 2023,https://doi.org/10.1109/ACCESS.2023.3273596

Tsuchiya, M., Nagahama, H., Muto, J., Hirano, M., and Yasuoka, Y.: Detection of atmospheric radon concentration anomalies and their potential for earthquake prediction using Random Forest analysis, Scientific Reports, 14, 11626, 2024,https://doi.org/10.1038/s41598-024-61887-6

https://doi.org/10.5194/egusphere-2026-1715
Preprint. Discussion started: 27 March 2026

Wang, Q., Guo, Y., Yu, L., and Li, P.: Earthquake prediction based on spatio-temporal data mining: an LSTM network approach, IEEE Transactions on Emerging Topics in Computing, 8, 148-158, 2017,https://doi.org/10.1109/TETC.2017.2699169

Wang, Q., Xu, X., Jiang, Z., and Suppe, J.: A possible precursor prior to the Lushan earthquake from GPS observations in the southern Longmenshan, Scientific Reports, 10, 20833, 2020,https://doi.org/10.1038/s41598-020-77634-6

Wang, w., Feng, Z., Zhu, P., Liao, X., He, C., and Zhang, Z.: Analysis of Pre-Earthquake Geomagnetic Disturbance Anomalies Prior to the MS6.0 Earthquake in Luxian County, Sichuan Province on 16 September 2021, Journal of Earthquake Engineering, 47, 229-239, 2025,https://doi.org/10.20000/j.1000-0844.20230410001.https://link.cnki.net/doi/10.20000/j.1000-0844.20230410001

Wang, Y., Li, J., Liu, L., and Fen, B.: Analysis of Tectonic Activity Characteristics of the 2013 Lushan 7.0-Magnitude Earthquake, PLATEAU EA R THQUAKE R ESEA R CH, 31, 20-25, 2019,https://doi.org/.https://kns.cnki.net/kcms2/article/abstract?v=z8lpvlhA63HIuaml_bCBk1INSQtx_jRp6cb6-kZ9mxrQrH3OPAGF5TGaBGrzuTOWJTPdinZy3zFPG4KaxCBR6LKSBod581Yvn0qKPJzJLMKjJY3qFcZiUCZ8bhisQnoXPDnZTBYrowl-avC6ih76oAdW0_-HSUIKgdt6sErLGpHApZrvI-igsHT4EBq0m_LT&uniplatform=NZKPT&language=CHS

Wu, A.: Group Substatistics and Quantitative Simulation of Drilling Strain Time Series, The 31st Chinese Conference on Control, 2012,https://doi.org/.https://kns.cnki.net/kcms2/article/abstract?v=W-y7fKBVJCyoXKqXX7BFuuP5-JGXy8zzCP-cowJdyYHM3eMkrvNBapNj_FS7lBKQaWWt3ZFJN8hh84O1bLlcEgj_SsRSBnM6FDjWlkT7MHYUjDX8CaD4iMZI77lyMITUebuuIbs_HDRjo-l-2GKwlb9In0mCoywxRyUCFVrvUBo=&uniplatform=NZKPT&language=CHS

Yang, P., Sun, X., Liu, D., He, Z., and Li, Y.: Hydrochemical characteristics of groundwater at the epicenter of the 2021 biru M6. 1 earthquake in central tibet, Water, 13, 3111, 2021,https://doi.org/10.3390/w13213111

Yang, Z. and Zhao, M.: On the Hazards and Prevention of Earthquake Disasters, Science and Technology & Innovation, 145-146, 2014,https://doi.org/10.15913/j.cnki.kjycx.2014.08.007

Ye, Q., Singh, R. P., He, A., Ji, S., and Liu, C.: Characteristic behavior of water radon associated with Wenchuan and Lushan earthquakes along Longmenshan fault, Radiation Measurements, 76, 44-53, 2015,https://doi.org/10.1016/j.radmeas.2015.04.001

Yu, Z., Jiang, Y., Jing, X., and Zheng, H.: Study on geomagnetic observations associated with three major earthquakes in Southwest China through a novel deep learning framework, IEEE Transactions on Geoscience and Remote Sensing, 2024,https://doi.org/10.1109/TGRS.2024.3411705

Yu, Z., Hattori, K., Zhu, K., Chi, C., Fan, M., and He, X.: Detecting earthquake-related anomalies of a borehole strain network based on multi-channel singular spectrum analysis, Entropy, 22, 1086, 2020,https://doi.org/10.3390/e22101086

Zhang, B., Yang, C., Zheng, H.-H., Yan, J.-Y., and Ma, C.-Y.: Geomagnetic Data Denoising Based on Deep Residual Shrinkage Network, Applied Geophysics, 22, 820-834, 2025a,https://doi.org/10.1007/s11770-025-1297-6

Zhang, X., De Santis, A., Liu, J., Campuzano, S. A., Yang, N., Cianchini, G., Ouyang, X., D'Arcangelo, S., Yang, M., and De Caro, M.: Pre-earthquake oscillating and accelerating patterns in the lithosphere–atmosphere–ionosphere coupling (LAIC) before the 2022 Luding (China) Ms6. 8 earthquake, Remote Sensing, 16, 2381, 2024,https://doi.org/10.3390/rs16132381

Zhang, Y., Huang, H., and Cheng, X.: Thermal anomaly detection for 2013 Lushan earthquake, 2016 IEEE International Geoscience and Remote Sensing Symposium (IGARSS), 2849-2852, https://dor.org/10.1109/IGARSS.2016.7729736

Zhang, Y., Zhou, H., Li, X., and Zhang, Z.: Remote sensing of latent heat flux anomalies in earthquake prediction, International Conference on Remote Sensing, Surveying, and Mapping (RSSM 2025), 279-284, https://dor.org/10.1117/12.3066576

Zhang, Z. and Wang, Y.: A global earthquake prediction model based on spherical convolutional LSTM, IEEE Transactions on Geoscience and Remote Sensing, 62, 1-10, 2024, https://doi.org/10.1109/TGRS.2024.3380573

Zhu, K., Chi, C., Yu, Z., Fan, M., Li, K., and Sun, H.: The characteristics analysis of strain variation associated with Wenchuan earthquake using principal component analysis, Annals of Geophysics, 63, PA549-PA549, 2020,https://doi.org/10.4401/ag-7946